Structure and Stability of 7-mercapto-4-methylcoumarin SAM on Gold: an Experimental and Computational analysis.

Davide Marchi,[‡] Eleonora Cara,[¶] Federico Ferrarese Lupi,[¶] Philipp Hönicke,[§] Yves Kayser,[§] Burkhard Beckhoff,[§] Micaela Castellino,[‖] Alberto Zoccante,[‡] Michele Laus,[‡] and Maurizio Cossi*[,‡]

‡*Dipartimento di Scienze e Innovazione Tecnologica (DISIT), Università del Piemonte Orientale, via T. Michel 11, I-15121, Alessandria, Italy*

¶*Istituto Nazionale di Ricerca Metrologica (INRIM), Strada delle Cacce, 91, I-10135, Torino, Italy*

§*Physikalisch-Technische Bundesanstalt (PTB), Abbestr. 2-12, 10587 Berlin, Germany.*

‖*Department of Applied Science and Technology, Politecnico di Torino, C.so Duca degli Abruzzi 24, 10129 Turin, Italy*

E-mail: maurizio.cossi@uniupo.it

Abstract

Self-assembled monolayers of 7-mercapto-4-methylcoumarin (MMC) on a flat gold surface were studied by Molecular Dynamics (MD) simulations, reference-free grazing incidence X-ray fluorescence (GIXRF) and X-ray pho-

toemission spectroscopy (XPS), to determine the maximum monolayer density and to investigate the nature of the molecule/surface interface. In particular, the protonation state of the sulfur atom upon adsorption was analyzed, since some recent literature presented evidences for physisorbed thiols (preserving the S-H bond), unlike the common picture of chemisorbed thiyls (losing the hydrogen). MD with a specifically tailored force field was used to simulate either thiol or thiyl monolayers with increasing number of molecules, to determine the maximum dynamically stable densities. This result was refined by computing the monolayer chemical potential as a function of the density with the Bennet Acceptance Ratio method, based again on MD simulations. The monolayer density was measured with GIXRF, which provided a quantitative estimate of the number of sulfur atoms on top of flat gold surfaces embedded in a solution of MMC, to allow the formation of a dense monolayer. The sulfur core level binding energies in the same monolayers were measured by XPS, fitting the recorded spectra with the binding energies proposed in the literature for free or adsorbed thiols and thiyls, to get insight on the nature of the molecular species present in the layer.

1 Introduction

Since their first description,[1] thiol self-assembled monolayers (SAM) on gold surfaces and nanoparticles have been widely used in a variety of technological applications,[2–13] and studied with a wealth of diffraction,[14–18] spectroscopic[8,19–23] and other surface science techniques.[24] In addition, thiol SAMs have been modeled theoretically by several ab initio (mainly density functional theory, DFT)[25–32] and molecular mechanics[27,28,33–38] studies.

Despite such a widespread interest, many key features of thiol/gold monolayers are still debated: even for some fundamental characteristics of the interface, as the

nature of sulfur-gold bond or the weight of intermolecular interactions inside the organic layer, different models have been proposed with no unique interpretation of the experimental data. For instance, the protonation state of the sulfur atom bonded to the metal surface is not unanimously accepted:[30,32,39] though most researchers assume that the S-H bond is dissociated and de-protonated sulfur is covalently bound to gold atoms,[2,40–42] some evidences have been presented showing that the layers can also be formed by undissociated thiol molecules.[43–46] (The former model is also referred to as "chemisorption", in contrast with the latter described as "physisorption" to stress the absence of a typical covalent bond between protonated sulfur and gold).

The present work contributes to this investigation, comparing the structure and stability of different SAMs of 7-mercapto-4-methylcoumarin (MMC) on gold (111) surfaces. A number of monolayers, formed either by undissociated thiol or radical thiyl MMC units (Figure 1), have been modeled theoretically, and the results compared with the absolute quantification of MMC surface density obtained by means of reference-free grazing incidence X-ray fluorescence (GIXRF) in SAMs prepared on 100 nm-thick gold layers. Additional X-ray photoelectron spectroscopy (XPS) characterization was performed to determine the nature of the thiol/thiyl S-Au chemical bond.

(A note on the terminology: since nearly all the proposed models for the dissociation of the S-H bond are based on a homolytic cleavage, eventually leading to H_2 formation, we prefer to consider the dissociated species as a radical thiyl rather than a thiolate ion, unlike many published studies. Whether the R-S unit has to be seen as a radical or an ion depends on the charge distribution in the S-Au bond, and appears as a rather unessential question in this context.)

Figure 1.

2 Methods and models

2.1 Theoretical modeling

Some models of thiol and thiyl SAM with different densities were prepared, to study their kinetic and thermodynamic stability with molecular dynamics (MD); the force fields (FF) were specifically parameterized for MMC on gold surfaces. Our goal is to determine the highest stable density and evaluate the chemical potential and the order degree for SAMs of both species: if thiol and thiyl SAM models exhibit different characteristics, the comparison with the experiments performed on the same system could shed some light on the protonation state of the sulfur atoms and in general on the structure of the SAM.

The gold (111) surface was modeled by cleaving a three layers thick slab out of the metal bulk structure: the periodic unit cell comprises 24×24 atoms in each layer and its surface area, considering an atomic radius for gold of 0.1385 nm, is 38.2 nm^2. MMC thiol and thiyl structures were optimized at the DFT level (with B3LYP/cc-pvDZ functional and basis), and a variable number of such units were assembled on the slab using PACKMOL package,[47] to create monolayers with the desired densities; in the initial conformations, all the organic units were in 'vertical' position (see below).

The FF parameters for MMC and ethanol were taken from GROMOS 54A7 set[48] as provided by the Automated Topology Builder (ATB) website; interactions of MMC molecules and radicals with the gold surface were described with pairwise non-bonding parameters fitted on DFT calculations as detailed in the Electronic Supporting Information (ESI). We decided to model both $-\mathrm{SH}\cdots\mathrm{Au}$ and $-\mathrm{S}\cdots\mathrm{Au}$ interactions with $6-12$ Lennard-Jones functions, though the latter can be considered a real covalent bond, to allow thiyl units to shift on the surface and possibly also leave too crowded monolayers.

All the FF-based calculations were carried out with GROMACS2020 package.[49] After an initial energy minimization, to remove spurious close contacts, the MD simulations were performed with 2×10^5 steps of 0.5 fs for equilibration, and 2×10^6 steps of 1 fs for production runs. A 3 nm cut-off was used for the Van der Waals

interactions, while electrostatic interactions were computed with a 2 nm cut-off, and using the PME method for longer distances; during all the simulations, Au positions were kept frozen.

The MMC chemical potential in the monolayers at various densities was computed as the free energy of decoupling[50] of one thiol or thiyl from the gold slab and the rest of the layer, using the Bennet Acceptance Ratio (BAR) method[51] implemented in GROMACS (gmx BAR procedure). Following this procedure, a coupling parameter λ (varying from 1 to 0 as the system shifts from real to decoupled) was defined to gradually switch off the intermolecular interactions between the target molecule and the rest of the system: first, Coulomb interactions were removed in 20 steps while vdW interactions remained unaltered, then also vdW terms were eliminated in 20 further steps, until the target unit was completely decoupled. For each λ value, a MD run was performed comprising 0.5 ns equilibration (timestep 0.5 fs) and 1 ns production (timestep 1 fs). The same procedure was adopted to compute the thiol free energy in ethanol solution.

2.2 Sample preparation

The preparation of the MMC SAM was conducted by following a standardized protocol.[52] The molecules of 7-mercapto-4-methylcoumarin were purchased in powder form from Merck. A solution of MMC in ethanol was prepared in the volume of 20 ml per each sample. The substrate preparation required cutting and cleaning pieces of a silicon wafer in ultrasonic bath with acetone and then isopropanol. A layer of 100 nm of gold was deposited on the substrates by means of RF sputtering in argon plasma with residual pressure of $5 \cdot 10^3$ mbar and power of 100 W. The resulting gold surface is continuous and polycrystalline. The gold-coated substrates were then immersed in the MMC solution for two hours, then abundantly rinsed with EtOH to remove any excess molecules not bounded to the gold surface.

2.3 GIXRF characterization

The quantitative characterization of the areal density of MMC molecules by reference-free grazing incidence X-ray fluorescence (GIXRF)[53] was conducted at the four crystal monochromator (FCM) beamline for bending magnet radiation[54] at the BESSY II synchrotron radiation facility. The reference-free GIXRF experiments were performed employing in-house built instrumentation,[55] which allows for precise sample alignment and angular variations of the sample with respect to the incident photon beam.

To optimize the excitation conditions for sulfur K-shell X-ray fluorescence, while minimizing the contributions of Au M-shell X-ray fluorescence to the experimental spectra, an incident photon energy of $E_0 = 2.6$ keV was chosen. During the GIXRF scans, the angle of incidence (defined between sample surface and incident X-ray beam) was varied between 0° and 7° with varying stepsize. At each angular position, a fluorescence spectrum was recorded by means of a calibrated[56] silicon drift detector (SDD) mounted at 90° with respect to the incident beam. Additional calibrated photodiodes on a separate 2θ axis allow for both X-ray reflectometry (XRR) measurements as well as for a determination of the incident photon flux. The recorded spectra are deconvolved using detector response functions[56] for relevant fluorescence lines and for background contributions as bremsstrahlung.

A SI-traceable quantification of the mass deposition of sulfur can be performed using the deconvoluted sulfur fluorescence events as presented in references 57,58. Using Sherman's equation[59] and necessary experimental parameters, e.g., the solid angle of detection or the incident photon flux, as well as atomic fundamental parameters, the mass deposition of sulfur can be calculated in absolute terms from the sulfur K X-ray fluorescence count rate as obtained from the spectral deconvolution. The required instrumental parameters are known due to the use of the well-known physically calibrated instrumentation.[58] The relevant fundamental parameters are taken from databases.[60] Here, the mass deposition of sulfur was quantified with an overall uncertainty of 11%, deriving mainly from the fundamental parameter uncertainties.

2.4 XPS characterization

A PHI 5000 Versaprobe Scanning X-ray Photoelectron Spectrometer (Physical Electronics, Chanhassen, MN, USA) has been involved in this study to get information regarding the relative atomic concentration (at.%) of each element present on the surface of both bare and functionalized Au thin film, and also to have further evidence regarding the bonds established between the MMC molecule and the golden surface. XPS measurements have also been carried out on MMC commercial powder, to check its bare chemical composition as a reference. The X-ray source was a monochromatic Al Kα radiation (1486.6 eV, 15 kV voltage and 1 mA anode current). All samples were subjected to a combined electron and Ar ion gun neutralizer system, to decrease the electrical charging effect during the analysis.

The semi-quantitative atomic concentration and fitting procedures were acquired using CasaXPS 2.3.23 dedicated software (Casa Software Ltd.,Wilmslow, UK). All core-level peak energies were referenced to C1s peak at 284.5 eV and the background contribution in HR scans was subtracted by means of a Shirley function. A spot size of 100 μm was used to collect the photoelectron signal for both the high resolution (HR) and the survey spectra.

Different pass energy values were employed: 187.8 eV for survey spectra and 23.5 eV for HR peaks. Survey scans (from 1200 to 0 eV, energy step ΔE = 0.1 eV) have been performed as the first step measurements to detect all the elements on sample surfaces. HR scans have been performed only in smaller ranges in the Binding Energy (BE) scale (energy step ΔE = 1 eV) around chemical element peaks of major interest for this study, i.e. C(1s), O(1s), S(2p) and Au(4f).

Powder sample has been loaded directly on a steel mask by attaching it on a double-sided conductive tape. Au thin film deposited on Si substrates (both functionalized with MMC molecule and not) have been attached on the 2-inches sample holder surface by means of double-sided conductive tape. Working pressure, inside the main chamber, has reached a maximum value of 10^{-6} Pa.

3 Results and discussion

3.1 Molecular dynamics modeling

Several models were defined placing an increasing number of thiol or thiyl units randomly onto the gold slab: then, after a MM minimization to remove close-contacts and spurious structures, MD simulations were run at 298 K until equilibration, and then for further 2 nm dynamics to check the monolayer stability. In the densest layers some of the organic molecules or radicals detached from the slab during the dynamics, remaining in contact with the other MMC units, in a sort of disordered double layer. We consider that such molecules, not interacting with the gold surface, would be washed away during the SAM preparation, so did not include them in the calculation of the SAM density.

The densities of the dynamically stable layers are collected in Table 1. Thiyls can be packed more closely than thiols, forming denser SAMs, as expected for their much larger interaction energy with gold, which balances the intermolecular repulsions in the crowded layers. Only when 216 thiyl units are initially placed on the surface, some of them are forced to leave the monolayer during the MD, while with thiols we find some units leaving the SAM even with 81 initial molecules. Clearly, the number of units expelled from the layer depends on the starting conformation also, but this effect becomes less important as the initial number grows and most of the surface is covered by the organic units: in fact, no attempt to start with more than 162 thiols or 216 thiyls led to densities larger than those reported in Table 1.

Table 1.

Besides investigating the density limit of stable monolayers, MD provides useful insights also about the SAM structure at various coverages. Apart from the units leaving the surface at high densities, mentioned above, molecules and radicals were found either in 'horizontal' or 'vertical' arrangement: in the former the units lie down on the slab maximizing the interaction of all the atoms with the surface, in the latter sulfur interacts strongly with gold, while the rest of the organic atoms are involved mainly in side intermolecular interactions, which can be overall attractive or repulsive, depending on the SAM density.

Some representative snapshots of the simulated thiol and thiyl SAMs are shown in Figures 2 and 3, respectively: clearly the position and orientation of the organic units change during the dynamics, but we found that the number of horizontal and vertical arrangements at the various densities is remarkably stable at 298 K.

Figure 2.

Figure 3.

The simulations show that at low coverage the organic units prefer to lie on the surface, because the interactions with the gold atoms are favored with respect to the intermolecular ones. As the SAM density increases, more and more molecules and radicals stand vertically, in agreement with the mechanism of the monolayer formation often proposed in the literature.[61–64] Thiol SAMs are less ordered then thiyl layers: in the former numerous molecules remain in horizontal position even at high densities competing with their vertical counterparts for the gold surface. As noted above, it is not possible to simulate an all-vertical thiol SAM, since the molecules prefer to leave a too crowded layer.

On the other hand, the vertical arrangement is easier in thiyl SAMs, since it allows a better interaction between the sulfur and gold atoms (which is markedly stronger than the analogous interaction in thiols) compensating the partial loss of stabilization when the molecule/surface interactions are substituted by side-side intermolecular ones. As a consequence, thiyl SAMs can be denser and more ordered: at high densities, almost all the radicals are in vertical position, allowing a closer packing. A picture of the ordered patterns established in a dense thiyl SAM, with several MMC phenyl rings stacked in lines is shown in the ESI.

3.2 Chemical potential calculations

The MD simulations discussed above provide useful insights about the SAM dynamical stability: however, this approach is not completely satisfactory for two reasons. First, the dynamics risk to be biased by the initial conformations, unless they can be run for a very long time and possibly with reasonable temperature annealings, to refine the exploration of the potential surfaces. A second, more severe problem is that during the MD the organic units can leave the monolayer "evaporating" into a

sort of low density gas phase, unlike in the real process of SAM formation, where the equilibrium establishes between the monolayer and a liquid thiol solution. Running the MD inside a box of solvent molecules did not solve the problem, for the strong cage effect hampering the detachment of thiols from the surface: moreover, when thiyl SAMs are involved, the -SH dissociation is also to be considered, as detailed below.

For these reasons, the information obtained with MD was complemented by the calculation of the monolayer chemical potentials as a function of the SAM density. The chemical potentials $\mu_{SH}(n),\ \mu_S(n)$ are defined as the free energy changes associated to the following processes:

$$\text{R-SH}_{(sol)} + \text{Au} \cdot (\text{R-SH})_{n-1} \longrightarrow \text{Au} \cdot (\text{R-SH})_n \ ; \qquad \mu_{SH}(n) \qquad (1)$$

$$\text{R-SH}_{(sol)} + \text{Au} \cdot (\text{R-S})_{n-1} \longrightarrow \text{Au} \cdot (\text{R-S})_n + \frac{1}{2}\ \text{H}_{2(g)} \ ; \qquad \mu_S(n) \qquad (2)$$

The number of organic units attached to the model slab after the reaction, from which the SAM density is computed, is n; following the experimental conditions, the reactant thiol is dissolved in ethanol, while the surface monolayer is considered in vacuo; in the case of thiyl SAM, the reaction includes the homolytic dissociation of the S-H bond and the formation of gaseous molecular hydrogen.

Then, to obtain the chemical potentials, we have to model the following elementary processes, combining the respective ΔGs:

$$\text{R-SH}_{(sol)} \longrightarrow \text{R-SH}_{(g)} \ ; \qquad \Delta G_{evap} \qquad (3)$$

$$\text{R-SH}_{(g)} \longrightarrow \text{R-S}_{(g)} + \frac{1}{2}\ \text{H}_{2(g)} \ ; \qquad \Delta G_{diss} \qquad (4)$$

$$\text{R-SH}_{(g)} + \text{Au} \cdot (\text{R-SH})_{n-1} \longrightarrow \text{Au} \cdot (\text{R-SH})_n \ ; \qquad \Delta G_{SH,g}(n) \qquad (5)$$

$$\text{R-S}_{(g)} + \text{Au} \cdot (\text{R-S})_{n-1} \longrightarrow \text{Au} \cdot (\text{R-S})_n \ ; \qquad \Delta G_{S,g}(n) \qquad (6)$$

Reactions 3 and 4 refer to the formation of molecular or radical units in the gas phase; 5 and 6 to the passage of one unit from the gas phase to thiol or thiyl

monolayers, respectively. With these definitions, the chemical potentials result:

$$\mu_{SH}(n) = \Delta G_{evap} + \Delta G_{SH,g}(n) \tag{7}$$

$$\mu_{S}(n) = \Delta G_{evap} + \Delta G_{diss} + \Delta G_{S,g}(n) \tag{8}$$

Reaction 4 was modeled at the DFT level with Gaussian16 program, including the calculation of vibrational frequencies and the evaluation of thermal contributions to enthalpy and entropy by classical Boltzmann averages; the selection of the suitable density functional and basis set, however, required some care. Since experimental data on S-H bond dissociation in MMC are not available, we collected the experimental values for benzenethiol and some of its derivatives, to evaluate the effect of both electron-withdrawing and electron-donating substituents, and computed ΔG_{diss} for these molecules with two hybrid (B3LYP, B3P86) and one pure (BLYP) functionals and a number of different basis sets. The DFT results are reported and analyzed in detail in the ESI: in conclusion, our best estimate is $\Delta G_{diss} = 130.0$ kJ/mol.

For the other steps we used the thermodynamic integration described in the "Methods and models" Section, which provides ΔG values with a series of MD simulations. This procedure was applied first to the evaporation of one MMC molecule from a box of ethanol molecules, reproducing the solvent density, and the free energy associated to reaction 3 resulted $\Delta G_{evap} = 17.9$ kJ/mol.

$\Delta G_{SH,g}(n)$ and $\Delta G_{S,g}(n)$ were computed with the thermodynamic integration method as well, decoupling one organic unit from each of the SAMs previously modeled and equilibrated with MD: the values obtained for thiol and thiyl at the various densities are collected in Table 2. Combining these results with the evaporation and dissociation free energies reported above, one finally obtains the SAM chemical potentials also reported in Table 2.

Table 2.

The data show that the chemical potential of thiol SAMs remains negative also at the highest densities attainable with the MD equilibration, which is mainly due to the large negative values of $\Delta G_{SH,g}$. One could wonder why it is not possible to

simulate SAMs with higher density, then: as mentioned above, when the monolayer initial density grows, an increasing number of thiols leave the gold surface during the MD and form a sort of second layer, strongly interacting with the underlying molecules still in the SAM. The free energy of these second layer thiols with respect to vacuum, computed with the same technique, falls in the range $102 - 112$ kJ/mol, depending on the position, very close to the $\Delta G_{SH,g}$ of thiols in the SAMs with 100 to 145 molecules. Then the dynamical instability of denser SAMs, observed above, can derive from the competition of the second layer, favoring the shift from the crowded SAM to the spacious layer floating above it.

On the other hand, in the case of thiyl layers we see that the densest SAMs, with 162 and 185 radicals on the model slab, are not thermodynamically favored, though stable during the MD. In fact, with $n = 162$ the free energy of insertion of one radical in gas phase ($\Delta G_{S,g}$) is still negative, but once considering the solvation and dissociation free energies, the chemical potential gets positive; even worse the situation for $n = 185$, where $\Delta G_{S,g}$ is already positive and is further increased by the other contributions. The system with 155 initial thiyls is borderline, as the computed chemical potential turns out very close to zero, even if $\Delta G_{S,g}$ is strongly negative: the result depends mainly on the large dissociation energy, whose calculation is quite approximated, as explained in the ESI, so the thermodynamic stability of this system is uncertain.

A further comment can be done about the system with 185 thiyls, where the strongly positive $\Delta G_{S,g}$ suggests a thermodynamically unstable SAM even without considering the de-solvation and bond dissociation contributions. Evidently, in this case the MD could not lead to a complete equilibration, since no radicals left the surface despite the thermodynamic advantage that could have been gained, because of the very high energy needed to break the strong S-Au bond, which "trapped" the SAM in a less favorable conformation. This is a good example of how the chemical potential calculation can refine the MD analysis.

3.3 Experimental quantification of the molecular density

The surface density of the MMC molecules in the SAMs formed on a flat reflecting gold surface was determined by performing a reference-free GIXRF experiment,[53] sketched in Figure 4a.

Figure 4.

In this analytical method, the angle of incidence of the X-ray beam is varied around the critical angle for total external reflection allowing the formation of an X-ray standing wave (XSW) interference field just above the sample surface. The XSW field enhances the fluorescence emitted by the atom inside it, while reducing the fluorescence signal from the substrate and thus spectral background.[57] The quantification can be performed, without any calibration standard, through the convertion of the element-specific fluorescence photon count rate $P_{\mathrm{e,K}}$ to the mass of the element of interest per unit area σ_{e} by combining the atomic fundamental parameters and calibrated instrumental parameters in the following equation.[59]

$$\sigma_{\mathrm{e}} = P_{\mathrm{e,K}} \cdot \frac{\sin\theta}{\Phi_0 \cdot \Omega/4\pi} \cdot \frac{1}{\epsilon_{(\mathrm{E_{e,K}})} \cdot I_{\mathrm{XSW}}(\mathrm{E}_0, \theta)} \cdot \frac{1}{\tau_{\mathrm{e,K}}(\mathrm{E}_0) \cdot \omega_{\mathrm{e,K}}} \tag{9}$$

where σ_{e} is expressed in g/cm^2. The radiometrically calibrated instrumental parameters correct the fluorescence photon count rate $P_{\mathrm{e,K}}$ obtained through spectral deconvolution (Figure 4b), i.e. the sine of the incidence angle θ, the incident photon flux Φ_0, the solid angle of detection $\Omega/4\pi$. The second correction factor accounts for the SDD's detection efficiency at the photon energy of the fluorescence line K for the element e and the incident photon energy E_0 and angular dependent relative intensity of the XSW field.[65] Finally, the fundamental parameters $\tau_{\mathrm{e,K}}(\mathrm{E}_0)$ and $\omega_{\mathrm{e,K}}$ are the partial photoionization cross section and fluorescence yield related to the K-shell of the target atom e, respectively. They form the production cross section for fluorescence radiation of the element of interest.

In the case of MMC, the GIXRF measurements were perfomed by selecting sulfur as target element. The experiment was carried out on a gold-coated substrate incubated in the MMC solution to determine the sulfur mass per unit area ascribable to the SAM. On each probed sample, the determined fluorescence photon count rate

of the sulfur K fluorescence line was converted to its mass per unit area using tabulated values of the sulfur K-shell fluorescence yield $\omega_{S,K} = 0.08038$ with a relative uncertainty of 7.5% estimated in reference 66 and of the partial photoionization cross section $\tau_{S,K}(E_0 = 2.6\ \text{keV}) = 1737\ \text{cm}^2\text{g}^{-1}$ with a relative uncertainty of 5%.[60]

The mass of sulfur per unit area was found to be $\sigma_{S_{MMC}} = (24.3 \pm 4.0)\ \text{ng/cm}^2$ and the same evaluation was performed on a bare gold sample where $\sigma_{S_{blank}} = (2.7 \pm 0.3)\ \text{ng/cm}^2$ of sulfur were detected. The amount of sulfur ascribable to the SAM was found by $\sigma_{S_{SAM}} = \sigma_{S_{MMC}} - \sigma_{S_{blank}} = (21.6 \pm 4.0)\ \text{ng/cm}^2$. The numerical density of sulfur atoms can be derived as $\sigma_{S_{SAM}} \cdot N_A / w_S$, where w_S is the atomic weight of sulfur and N_A Avogadro's number. Since there is only one sulfur atom per each molecule, its numerical density corresponds to the number of self-assembled molecules per unit area which is $(4.1 \pm 0.7)\ \text{nm}^{-2}$. The total uncertainty associated to every reported value is due to the propagation of uncertainties for independent variables including statistical uncertainty on repeated measurements and the uncertainty contributions in equation 9, i.e. the uncertainties on the fundamental atomic parameters, already reported, 4% relative uncertainty on the determination of solid angle of detection, 1.5% relative uncertainty on the incident photon flux and 2% on the XSW field intensity above the sample surface.

3.4 XPS analysis of the bond chemistry

The nature of bonds between gold surfaces and organic thiols has been widely studied in the last decades. XPS is one of the most used techniques to investigate such bonds, considering in particular the difference between bound and unbound species. As reported by Castner et al.,[67] there is a sort of hierarchical displacement in the position of the $S(2p_{3/2})$ core-level binding energy (CLBE), which follows this general trend: unbound thiol or disulfide (164-163 eV), bound thiol or thiyl in hollow site (162 eV) and thiyl in low-coordination site (< 162 eV). Zubragel et al.[68] have also deeply studied the presence of different sulfur species in SAMs on Au and Ag, but they attribute the chemical shift at 161.8 eV to threefold bound thiols, and the shift at 163.1 eV the bound thiyl in lower coordination sites, in contrast with the work in reference 67. More recent works have tried to describe more accurately the chemical species that can be found on a Au thin film, by comparing DFT simulations with

surface experimental analysis.[69–71] In particular, Jia et al.[71] have recognized four different chemical shifts due to the interaction of sulfur species on the Au layer. A first component at low binding energy (161.2 eV) is assigned to the thiyl in a metastable site rather than atomic sulfur, as previously reported,[69] a second one (162.0 eV) to bound thiyl, a third one (163.0 eV) to unbound or free -SH, and a final one at binding energy higher than 163.5 eV, is assigned to physisorbed -SH on a second layer on SAM.

Thus we have decided to check the MMC powder, which provides the reference value for unbound thiol, as well as the blank Au thin film deposited on Si, and the MMC SAM on Au thin film sample (see figure 5). MMC powder survey spectrum (not reported) has shown the presence of C(1s), O(1s) and S(2p) peaks, as expected, while the bare Au thin film and the MMC on Au samples have shown in addition the presence of Au(4f) doublet. The presence of S on the blank Au sample has been ascribed to environmental contamination, due to sulfur species present in the atmosphere. In figure 5, HR S(2p) core level spectra have been reported for the three analyzed samples, together with their deconvolution procedure.

Figure 5.

For the MMC SAM on Au sample we identify the following four components, each made up by a doublet due to S($2p_{3/2}$) and S($2p_{1/2}$) spin-orbit splitting (Figure 5a): i) at 161.0 eV (8.6%), ii) at 162.0 eV (58.9%), iii) at 163.1 eV (19.9%) and iv) at 163.7 eV (12.6%). On the other hand, for the blank gold surface we find three peaks (Figure 5b): i) at 161.3 eV (41.8%), ii) at 162.1 eV (43.6%) and iii) at 163.2 eV (14.6%); the fourth component at higher binding energy is missing in this core level peak deconvolution. For the MMC powder the detected peaks are further reduced, with only two components ((Figure 5c): i) at 163.1 eV (53.9%) and ii) at 163.7 eV (46.1%).

In agreement with Jia et al. assignments,[71] the components detected in the MMC powder are attributed to free -SH or mutually interacting thiols (referred to as "second layer" in the Figure caption). Passing to MMC SAM, two new, intense peaks arise at lower CLBE: most authors attribute the signals in this region to thiyls chemisorbed on the Au surface (often referred to in the literature as "thiolate", as noted above), though the possibility of physisorbed thiols is not definitely excluded.

Interestingly, the peaks due to free -SH above 163 eV are also present in the SAM photoemission spectra, even if weaker than the lower energy components, suggesting the presence of unbound species, possibly in the second layer mentioned above. The presence of signals from adsorbed and, to a lower extent, free sulfur species even in the Au blank confirms the environmental contamination already detected by XRF experiments.

3.5 Comparison of experimental and theoretical results

As seen above, the MD analysis of denser and denser SAMs allows to put an upper bound to the number of thiol or thiyl units that can be assembled on a flat, unreconstructed (111) gold surface: we found that the highest dynamically stable densities are 3.8 nm^{-2} for thiols, and 4.8 nm^{-2} for thiyls.

The calculation of SAM chemical potentials, obtained with MD thermodynamic integration and ab initio calculations, leads to a refinement of the previous conclusion for the thiyl monolayers: with this approach, the maximum density of thiol SAMs is confirmed at 3.8 nm^{-2} while for thiyl SAMs it results not higher than 4.1 nm^{-2}. The strong reduction of the maximum predicted density for thiyl SAMs is mainly due to the large dissociation energy of the S-H bond, which counterbalances the stronger interaction of the radicals with the surface. However, if the dissociation reaction were not completely equilibrated (for instance because the molecular hydrogen leaves the sample), the expected density for thiyl SAMs would be larger: this possibility will be examined in further studies.

The SAM density obtained from the GIXRF experiments is (4.1 ± 0.7) molecules/nm^{-2}, thus compatible with both the theoretical predictions for thiol or thiyl SAM within the error bar. Note that this value assumes that the sulfur species contaminating the blank Au sample remain on the surface even after the MMC adsorption: if these species were substituted by MMC, totally or in part, the final SAM density would result larger, with an upper bound of (4.6 ± 0.6) molecules/nm^{-2} (in the case that all the contaminants on the blank were substituted by MMC).

The XPS measurements performed on the same SAM allowed to probe the chem-

ical bond at the SAM interface, and to postulate the sulfur oxidation state. Two signals have been assigned to adsorbed radicals: the more intense one (58.9%) to thiyl group and the second one (8.6%) to metastable thiyl in alternative adsorption sites. Two weaker components have been ascribed to free or physisorbed thiol species, either at the Au surface or in a second layer above the MMC SAM.

In conclusion, the comparison of theoretical and experimental densities cannot indicate the sulfur protonation state unambiguously, even if further analyses (including e.g. non-equilibrated dissociation reactions and reduced contaminant effects in the GIXRF measures) could clarify the point better. On the other hand, the XPS analysis indicates the prevalence of radical thiyls adsorbed on the gold surface, though in the presence of a lesser component of undissociated thiols.

Electronic Supporting Information

The Supporting Information is available free of charge on the ACS Publications website at DOI:

Details on the FF parameterization, picture of high densiy thiyl SAM, calculation of S-H dissociation free energy.

Acknowledgement

D. M., A. Za,. M. L. and M. Co. acknowledge the financial support by Università del Piemonte Orientale (through the FAR-2019 funding program). E.C. F.F.L. P.H. Y.K. B.B. acknowledge the project 19ENV05 AEROMET II. The project 19ENV05 AEROMET II has received funding from the EMPIR programme co-financed by the Participating States and from the European Unions Horizon 2020 research and innovation programme.

References

(1) Nuzzo, R. G.; Allara, D. L. Adsorption of Bifunctional Organic Disulfides on Gold Surfaces. *J. Am. Chem. Soc.* **1983**, *105*, 4481–4483.

(2) Vericat, C.; Vela, M.; Benitez, G.; Carro, P.; Salvarezza, R. Self-assembled Monolayers of Thiols and Dithiols on Gold: New Challenges for a Well-known System. *Chem. Soc. Rev.* **2010**, *39*, 1805–1834.

(3) Häkkinen, H. The Gold-sulfur Interface At the Nanoscale. *Nat. Chem.* **2012**, *4*, 443–455.

(4) Laroussi, A.; Kot, M.; Flege, J.; Raouafi, N.; Mirsky, V. Self-assembled Monolayers from Symmetrical Di-thiols: Preparation, Characterization and Application for the Assembly of Electrochemically Active Films. *Appl. Surf. Sci.* **2020**, *513*, 145827.

(5) Rovati, D.; Albini, B.; Galinetto, P.; Grisoli, P.; Bassi, B.; Pallavicini, P.; Dacarro, G.; Taglietti, A. High Stability Thiol-coated Gold Nanostars Monolayers with Photothermal Antibacterial Activity and Wettability Control. *Nanomaterials* **2019**, *9*, 1288.

(6) Wang, Y.-S.; Yau, S.; Chau, L.-K.; Mohamed, A.; Huang, C.-J. Functional Biointerfaces Based on Mixed Zwitterionic Self-Assembled Monolayers for Biosensing Applications. *Langmuir* **2019**, *35*, 1652–1661.

(7) Pengo, P.; Pasquato, L. Gold Nanoparticles Protected By Fluorinated Ligands: Syntheses, Properties and Applications. *J. Fluor. Chem.* **2015**, *177*, 2–10.

(8) Lawton, T.; Uzarski, J.; Filocamo, S. A Multifunctional Surface That Simultaneously Balances Hydrophilic Enzyme Catalysis and Hydrophobic Water Repellency. *Chem. Eur. J.* **2016**, *22*, 12068–12073.

(9) Bhuvana, M.; Dharuman, V. Influence of Alkane Chain Lengths and Head Groups on Tethering of Liposome-gold Nanoparticle on Gold Surface for Electrochemical DNA Sensing and Gene Delivery. *Sens. Actuators B Chem.* **2016**, *223*, 157–165.

(10) Demirkol, D.; Yildiz, H.; Sayin, S.; Yilmaz, M. Enzyme Immobilization in Biosensor Constructions: Self-assembled Monolayers of Calixarenes Containing Thiols. *RSC Adv.* **2014**, *4*, 19900–19907.

(11) Crudden, C.; Horton, J.; Ebralidze, I.; Zenkina, O.; McLean, A.; Drevniok, B.; She, Z.; Kraatz, H.-B.; Mosey, N.; Seki, T.; Keske, E.; Leake, J.; Rousina-Webb, A.; Wu, G. Ultra Stable Self-assembled Monolayers of N-heterocyclic Carbenes on Gold. *Nat. Chem.* **2014**, *6*, 409–414.

(12) Valley, D.; Onstott, M.; Malyk, S.; Benderskii, A. Steric Hindrance of Photoswitching in Self-assembled Monolayers of Azobenzene and Alkane Thiols. *Langmuir* **2013**, *29*, 11623–11631.

(13) Newton, L.; Slater, T.; Clark, N.; Vijayaraghavan, A. Self Assembled Monolayers (SAMs) on Metallic Surfaces (gold and Graphene) for Electronic Applications. *J. Mater. Chem. C* **2013**, *1*, 376–393.

(14) Reik, M.; Calabro, M.; Griesemer, S.; Barry, E.; Bu, W.; Lin, B.; Rice, S. The Influence of Fractional Surface Coverage on the Core-core Separation in Ordered Monolayers of Thiol-ligated Au Nanoparticles. *Soft Matter* **2019**, *15*, 8800–8807.

(15) Azzam, W.; Cyganik, P.; Witte, G.; Buck, M.; Wöll, C. Pronounced OddEven Changes in the Molecular Arrangement and Packing Density of Biphenyl-Based Thiol SAMs: a Combined STM and LEED Study. *Langmuir* **2003**, *19*, 8262–8270.

(16) Heister, K.; Allara, D. L.; Bahnck, K.; Frey, S.; Zharnikov, M.; Grunze, M. Deviations from 1:1 Compositions in Self-Assembled Monolayers Formed from Adsorption of Asymmetric Dialkyl Disulfides on Gold. *Langmuir* **1999**, *15*, 5440–5443.

(17) Gerlach, R.; Polanski, G.; Rubahn, H.-G. Growth of Ultrathin Organic Films on Au(111) Surfaces. *Thin Solid Films* **1998**, *318*, 270–272.

(18) Whelan, C. M.; Barnes, C. J.; Walker, C. G.; Brown, N. M. Benzenethiol Adsorption on Au(111) Studied By Synchrotron ARUPS, HREELS and XPS. *Surface Science* **1999**, *425*, 195–211.

(19) Tirotta, I.; Calloni, A.; Pigliacelli, C.; Brambilla, A.; Bussetti, G.; Du, L.; Metrangolo, P.; Baldelli Bombelli, F. Chemical Characterization of Fluorinated/hydrogenated Mixed Monolayers Grafted on Gold Nanoparticles. *Journal of Fluorine Chemistry* **2018**, *206*, 99–107.

(20) Pick, A.; Witte, G. Patterned Growth of Organic Semiconductors: Selective Nucleation of Perylene on Self-Assembled Monolayers. *Langmuir* **2016**, *32*, 8019–8028.

(21) Pak, F.; Meral, K.; Altunda, R.; Ekinci, D. Self-assembled Monolayers of Fluorene- and Nitrofluorene-terminated Thiols on Polycrystalline Gold Electrode: Electrochemical and Optical Properties. *J. Electroanal. Chem.* **2011**, *654*, 20–28.

(22) Lewis, P. A.; Donhauser, Z. J.; Mantooth, B. A.; Smith, R. K.; Bumm, L. A.; Kelly, K. F.; Weiss, P. S. Control and Placement of Molecules Via Self-assembly. *Nanotechnology* **2001**, *12*, 231–237.

(23) Tai, Y.; Shaporenko, A.; Eck, W.; Grunze, M.; Zharnikov, M. Depth Distribution of Irradiation-Induced Cross-Linking in Aromatic Self-Assembled Monolayers. *Langmuir* **2004**, *20*, 7166–7170.

(24) Vericat, C.; Vela, M. E.; Benitez, G. A.; Gago, J. A. M.; Torrelles, X.; Salvarezza, R. C. Surface Characterization of Sulfur and Alkanethiol Self-assembled Monolayers on Au(111). *J. of Phys.: Condens. Matter* **2006**, *18*, R867–R900.

(25) Mhlanga, N.; Ntho, T. A Theoretical Study of 4-Mercaptobenzoic Acid Assembled

on Ag for Surface-enhanced Raman Scattering Applications. *Materials Today Communications* **2021**, *26*, 101698.

(26) Chadha, R.; Das, A.; Kapoor, S.; Maiti, N. Surface-induced Dimerization of 2-thiazoline-2-thiol on Silver and Gold Nanoparticles: a Surface Enhanced Raman Scattering (SERS) and Density Functional Theoretical (DFT) Study. *J. Mol. Liq.* **2021**, *322*, 114536.

(27) Engelbrekt, C.; Nazmutdinov, R.; Zinkicheva, T.; Glukhov, D.; Yan, J.; Mao, B.; Ulstrup, J.; Zhang, J. Chemistry of Cysteine Assembly on Au(100): Electrochemistry,: in Situ STM and Molecular Modeling. *Nanoscale* **2019**, *11*, 17235–17251.

(28) Roy, J.; Vasquez, E.; Pinto, H.; Kumari, S.; Walters, K.; Leszczynski, J. Computational and Experimental Approach to Understanding the Structural Interplay of Self-assembled End-terminated Alkanethiolates on Gold Surfaces. *Phys. Chem. Chem. Phys.* **2019**, *21*, 23320–23328.

(29) Herrera, S.; Tasca, F.; Williams, F.; Calvo, E.; Carro, P.; Salvarezza, R. Surface Structure of 4-Mercaptopyridine on Au(111): a New Dense Phase. *Langmuir* **2017**, *33*, 9565–9572.

(30) Guesmi, H.; Luque, N.; Santos, E.; Tielens, F. Does the SH Bond Always Break After Adsorption of An Alkylthiol on Au(111)? *Chem. Eur. J.* **2017**, *23*, 1402–1408.

(31) Peiretti, L.; Quaino, P.; Tielens, F. Competition Between Two High-density Assemblies of Poly(phenyl)thiols on Au(111). *J. Phys. Chem. C* **2016**, *120*, 25462–25472.

(32) Bedford, E.; Humblot, V.; Mthivier, C.; Pradier, C.-M.; Gu, F.; Tielens, F.; Boujday, S. An Experimental and Theoretical Approach to Investigate the Effect of Chain Length on Aminothiol Adsorption and Assembly on Gold. *Chem. Eur. J.* **2015**, *21*, 14555–14561.

(33) First, J.; Webb, L. Agreement Between Experimental and Simulated Circular Dichroic Spectra of a Positively Charged Peptide in Aqueous Solution and on Self-Assembled Monolayers. *J. Phys. Chem. B* **2019**, *123*, 4512–4526.

(34) Liu, X.; Lu, P.; Zhai, H.; Wu, Y. Temperature-dependent Surface Density of Alkylthiol Monolayers on Gold Nanocrystals. *Mater. Res. Express* **2018**, *5*, 035001.

(35) Sridhar, D.; Gupta, R.; Rai, B. Effect of Surface Coverage and Chemistry on Self-assembly of Monolayer Protected Gold Nanoparticles: a Molecular Dynamics Simulation Study. *Phys. Chem. Chem. Phys.* **2018**, *20*, 25883–25891.

(36) Meena, S.; Goldmann, C.; Nassoko, D.; Seydou, M.; Marchandier, T.; Moldovan, S.; Ersen, O.; Ribot, F.; Chanac, C.; Sanchez, C.; Portehault, D.; Tielens, F.; Sulpizi, M. Nanophase Segregation of Self-Assembled Monolayers on Gold Nanoparticles. *ACS Nano* **2017**, *11*, 7371–7381.

(37) Devi, J. Simulation Studies on Structural and Thermal Properties of Alkane Thiol Capped Gold Nanoparticles. *J. Mol. Graph. Model.* **2017**, *74*, 359–365.

(38) Rodríguez González, M.; Carro, P.; Pensa, E.; Vericat, C.; Salvarezza, R.; Hernández Creus, A. The Role of a Double Molecular Anchor on the Mobility and Self-Assembly of Thiols on Au(111): the Case of Mercaptobenzoic Acid. *ChemPhysChem* **2017**, *18*, 804–811.

(39) Luque, N. B.; Santos, E.; Andres, J.; Tielens, F. Effect of Coverage and Defects on the Adsorption of Propanethiol on Au(111) Surface: a Theoretical Study. *Langmuir* **2011**, *27*, 14514–14521.

(40) Tielens, F.; Santos, E. AuS and SH Bond Formation/Breaking During the Formation of Alkanethiol SAMs on Au(111): a Theoretical Study. *J. Phys. Chem. C* **2010**, *114*, 9444–9452.

(41) Rouhana, L. L.; Moussallem, M. D.; Schlenoff, J. B. Adsorption of Short-Chain Thiols and Disulfides Onto Gold Under Defined Mass Transport Conditions: Coverage, Kinetics, and Mechanism. *J. Am. Chem. Soc.* **2011**, *133*, 16080–16091.

(42) Kankate, L.; Turchanin, A.; Glzhuser, A. On the Release of Hydrogen from the SH Groups in the Formation of Self-Assembled Monolayers of Thiols. *Langmuir* **2009**, *25*, 10435–10438.

(43) Inkpen, M.; Liu, Z.; Li, H.; Campos, L.; Neaton, J.; Venkataraman, L. Non-chemisorbed Goldsulfur Binding Prevails in Self-assembled Monolayers. *Nat. Chem.* **2019**, *11*, 351–358.

(44) Rzeźnicka, I. I.; Lee, J.; Maksymovych, P.; Yates, J. T. Nondissociative Chemisorption of Short Chain Alkanethiols on Au(111). *J. Phys. Chem. B* **2005**, *109*, 15992–15996.

(45) Hasan, M.; Bethell, D.; Brust, M. The Fate of Sulfur-Bound Hydrogen on Formation of Self-Assembled Thiol Monolayers on Gold: 1H NMR Spectroscopic Evidence from Solutions of Gold Clusters. *J. Am. Chem. Soc.* **2002**, *124*, 1132–1133.

(46) Nuzzo, R. G.; Zegarski, B. R.; Dubois, L. H. Fundamental Studies of the Chemisorption of Organosulfur Compounds on Gold(111). Implications for Molecular Self-assembly on Gold Surfaces. *J. Am. Chem. Soc.* **1987**, *109*, 733–740.

(47) Martínez, L.; Andrade, R.; Birgin, E. G.; Martínez, J. M. PACKMOL: a Package for Building Initial Configurations for Molecular Dynamics Simulations. *J. Comput. Chem.* **2009**, *30*, 2157–2164.

(48) Schmid, N.; Eichenberger, A. P.; Choutko, A.; Riniker, S.; Winger, M.; Mark, A. E.; van Gunsteren, W. F. Definition and Testing of the GROMOS Force-Field Versions 54A7 and 54B7. *Eur. Biophys. J.* **2011**, *40*, 843856.

(49) Abraham, M. J.; Murtola, T.; Schulz, R.; Pll, S.; Smith, J. C.; Hess, B.; Lindahl, E. GROMACS: High Performance Molecular Simulations Through Multi-level Parallelism from Laptops to Supercomputers. *SoftwareX* **2015**, *1-2*, 19–25.

(50) Khanna, V.; Monroe, J. I.; Doherty, M. F.; Peters, B. Performing Solvation Free Energy Calculations in LAMMPS Using the Decoupling Approach. *J. Compu. Aided Molec. Des.* **2020**, *34*, 641–646.

(51) Bennett, C. H. Efficient Estimation of Free Energy Differences from Monte Carlo Data. *J. Comput. Phys.* **1976**, *22*, 245–268.

(52) Love, J. C.; Estroff, L. A.; Kriebel, J. K.; Nuzzo, R. G.; Whitesides, G. M. Self-assembled monolayers of thiolates on metals as a form of nanotechnology. *Chemical reviews* **2005**, *105*, 1103–1170.

(53) Hönicke, P.; Detlefs, B.; Nolot, E.; Kayser, Y.; Mühle, U.; Pollakowski, B.; Beckhoff, B. Reference-free grazing incidence x-ray fluorescence and reflectometry as a methodology for independent validation of x-ray reflectometry on ultrathin layer stacks and a depth-dependent characterization. *Journal of Vacuum Science & Technology A: Vacuum, Surfaces, and Films* **2019**, *37*, 041502.

(54) Krumrey, M.; Ulm, G. High-accuracy detector calibration at the PTB four-crystal monochromator beamline. *Nuclear Instruments and Methods in Physics Research Section A: Accelerators, Spectrometers, Detectors and Associated Equipment* **2001**, *467*, 1175–1178.

(55) Lubeck, J.; Beckhoff, B.; Fliegauf, R.; Holfelder, I.; Hönicke, P.; Müller, M.; Pollakowski, B.; Reinhardt, F.; Weser, J. A novel instrument for quantitative nanoanalytics involving complementary X-ray methodologies. *Review of Scientific Instruments* **2013**, *84*, 045106.

(56) Scholze, F.; Procop, M. Modelling the response function of energy dispersive X-ray spectrometers with silicon detectors. *X-Ray Spectrometry: An International Journal* **2009**, *38*, 312–321.

(57) Müller, M.; Hönicke, P.; Detlefs, B.; Fleischmann, C. Characterization of high-k nanolayers by grazing incidence X-ray spectrometry. *Materials* **2014**, *7*, 3147–3159.

(58) Beckhoff, B. Reference-free X-ray spectrometry based on metrology using synchrotron radiation. *Journal of Analytical Atomic Spectrometry* **2008**, *23*, 845–853.

(59) Sherman, J. The theoretical derivation of fluorescent X-ray intensities from mixtures. *Spectrochimica acta* **1955**, *7*, 283–306.

(60) Schoonjans, T.; Brunetti, A.; Golosio, B.; del Rio, M. S.; Solé, V. A.; Ferrero, C.; Vincze, L. The xraylib library for X-ray–matter interactions. Recent developments. *Spectrochimica Acta Part B: Atomic Spectroscopy* **2011**, *66*, 776–784.

(61) Ravi, V.; Binz, J. M.; Rioux, R. M. Thermodynamic Profiles At the Solvated InorganicOrganic Interface: the Case of GoldThiolate Monolayers. *Nano Lett.* **2013**, *13*, 4442–4448.

(62) Jung, L. S.; Campbell, C. T. Sticking Probabilities in Adsorption of Alkanethiols from Liquid Ethanol Solution Onto Gold. *J. Phys. Chem. B* **2000**, *104*, 11168–11178.

(63) Królikowska, A.; Kudelski, A.; Michota, A.; Bukowska, J. SERS Studies on the Structure of Thioglycolic Acid Monolayers on Silver and Gold. *Surf. Sci.* **2003**, *532-535*, 227–232.

(64) Poirier, G. E.; Pylant, E. D. The Self-Assembly Mechanism of Alkanethiols on Au(111). *Science* **1996**, *272*, 1145–1148.

(65) Soltwisch, V.; Hönicke, P.; Kayser, Y.; Eilbracht, J.; Probst, J.; Scholze, F.; Beckhoff, B. Element sensitive reconstruction of nanostructured surfaces with finite elements and grazing incidence soft X-ray fluorescence. *Nanoscale* **2018**, *10*, 6177–6185.

(66) Krause, M. O. Atomic radiative and radiationless yields for K and L shells. *Journal of physical and chemical reference data* **1979**, *8*, 307–327.

(67) Castner, D. G.; Hinds, K.; Grainger, D. W. X-ray photoelectron spectroscopy sulfur 2p study of organic thiol and disulfide binding interactions with gold surfaces. *Langmuir* **1996**, *12*, 5083–5086.

(68) Zubrägel, C.; Deuper, C.; Schneider, F.; Neumann, M.; Grunze, M.; Schertel, A.; Wöll, C. The presence of two different sulfur species in self-assembled films of n-alkanethiols on Au and Ag surfaces. *Chemical physics letters* **1995**, *238*, 308–312.

(69) Ishida, T.; Choi, N.; Mizutani, W.; Tokumoto, H.; Kojima, I.; Azehara, H.; Hokari, H.; Akiba, U.; Fujihira, M. High-resolution X-ray photoelectron spectra of organosulfur monolayers on Au (111): S (2p) spectral dependence on molecular species. *Langmuir* **1999**, *15*, 6799–6806.

(70) Dufour, F.; Fresch, B.; Durupthy, O.; Chanéac, C.; Remacle, F. Ligand and solvation effects on the structural and electronic properties of small gold clusters. *The Journal of Physical Chemistry C* **2014**, *118*, 4362–4376.

(71) Jia, J.; Kara, A.; Pasquali, L.; Bendounan, A.; Sirotti, F.; Esaulov, V. A. On sulfur core level binding energies in thiol self-assembly and alternative adsorption sites: An experimental and theoretical study. *The Journal of Chemical Physics* **2015**, *143*, 104702.

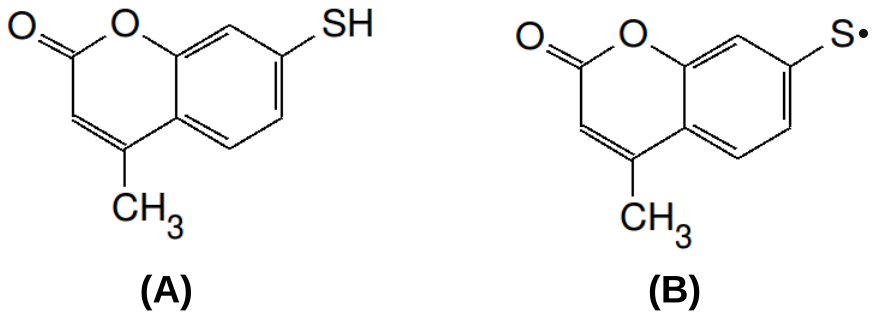

Figure 1: 7-mercapto-4-methylcoumarin (MMC) thiol molecule (A) and thiyl radical (B).

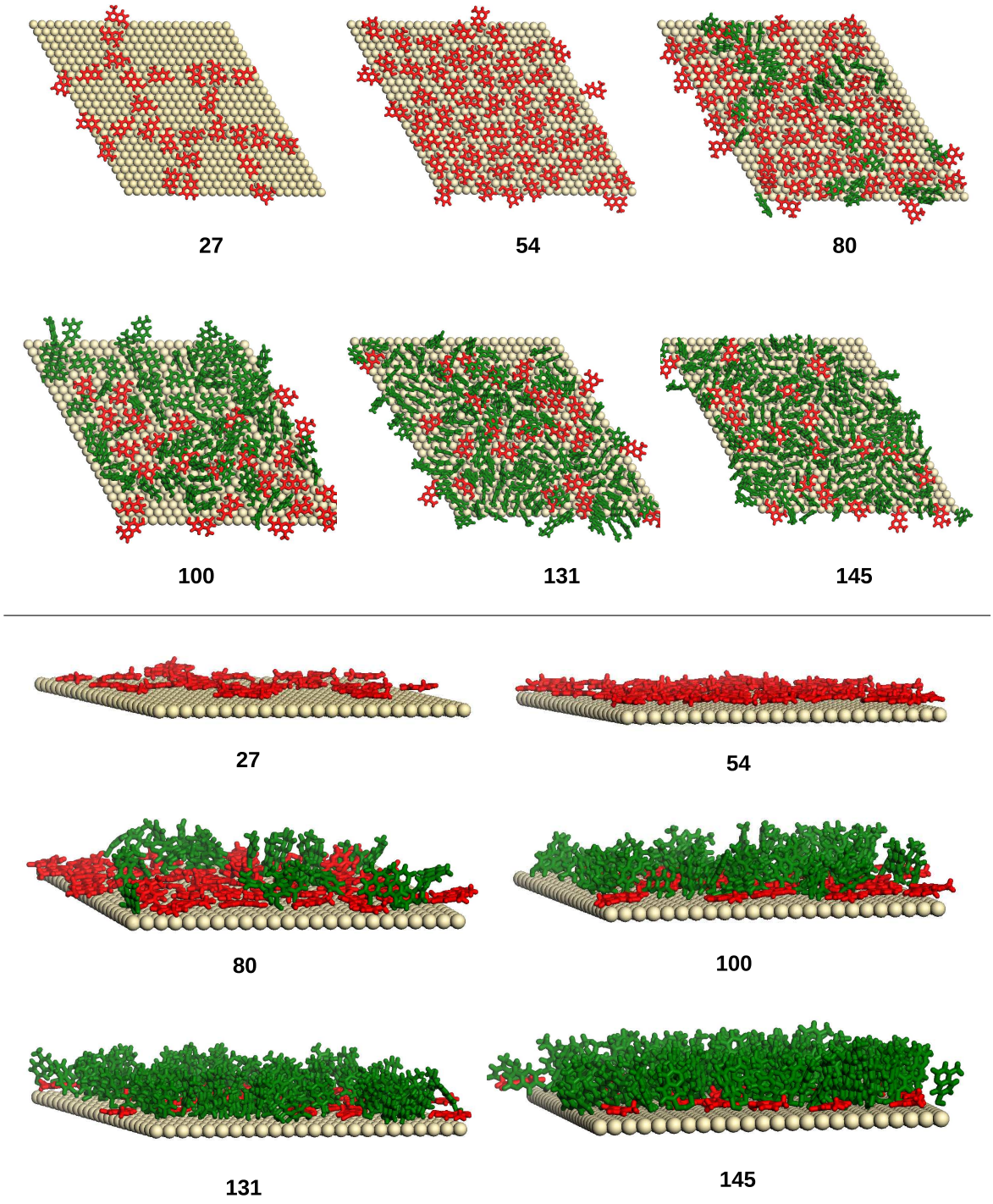

Figure 2: MD snapshots (top and side views) of thiol SAMs with different numbers of attached units (indicated below each image). In red/green molecules in horizontal/vertical arrangement.

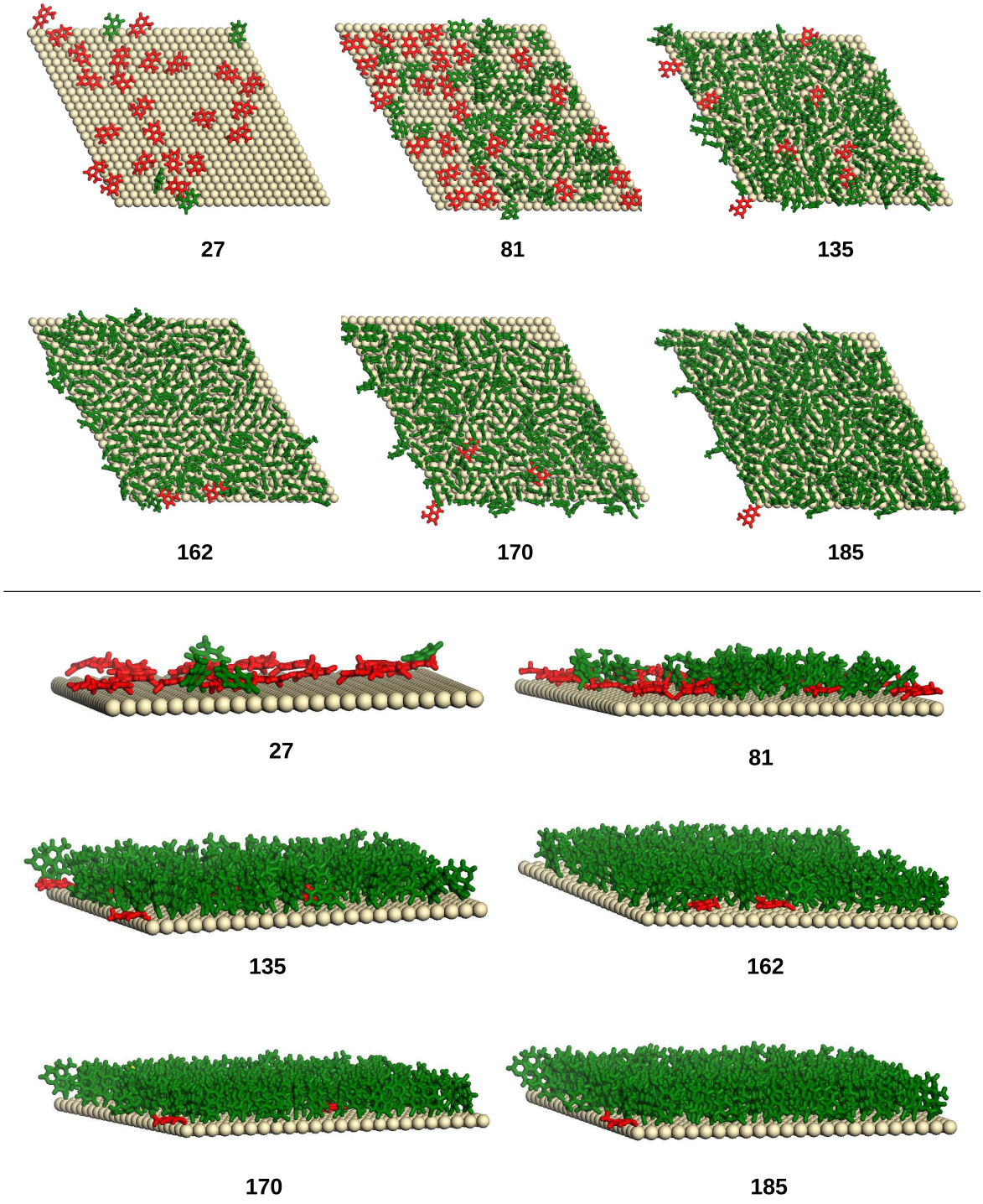

Figure 3: MD snapshots (top and side views) of thiyl SAMs with different numbers of attached units (indicated below each image). In red/green molecules in horizontal/vertical arrangement.

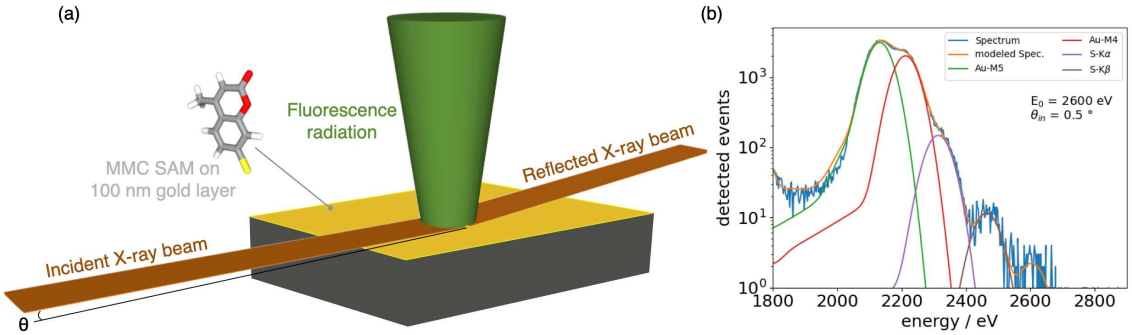

Figure 4: (a) Schematic representation of the GIXRF measurement where the X-ray beam impinges on the reflecting sample surface at θ angle and excites the fluorescence radiation detected at 90°. (b) Deconvolution of the spectrum acquired at $\theta = 0.5°$.

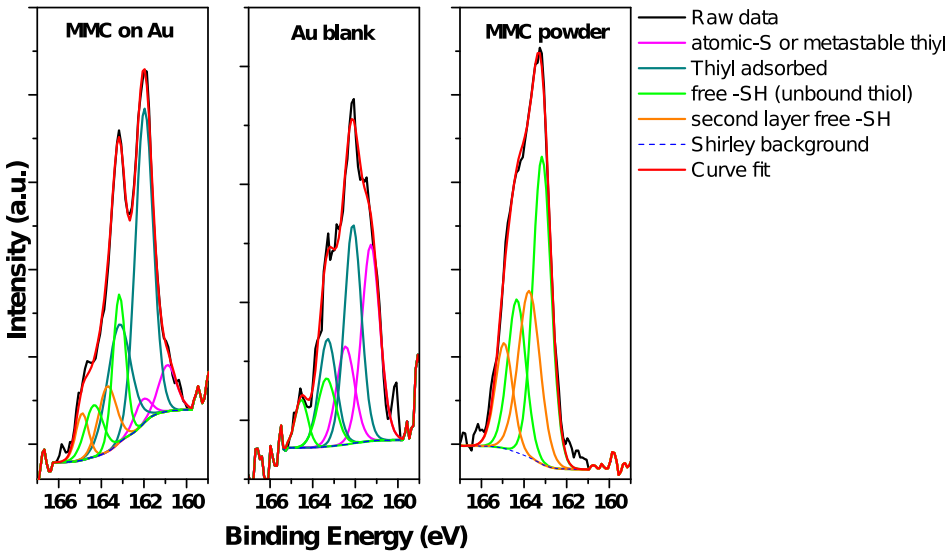

Figure 5: XPS S(2p) core level spectra for MMC SAM on Au (a), blank Au thin film (b) and MMC precursor powder (c). Deconvolution curves have been reported in each graph and their common legenda has been added aside.

Table 1: Number of molecules or radicals in the SAM and corresponding density (the gold slab area being 38.2 nm^2): when some units left the surface during the MD, the initial number is indicated in parentheses.

Thiol	# starting units	27	54	(81) → 75	(108) → 97	(135) → 126	(162) → 142
	density (nm^{-2})	0.71	1.41	1.96	2.54	3.30	3.72
Thiyl	# starting units	27	81	135	155	162	(216) → 185
	density (nm^{-2})	0.71	2.12	3.53	4.06	4.24	4.84

Table 2: Free energy of insertion in vacuo (ΔG_g, kJ/mol) and chemical potential (μ, kJ/mol) of MMC monolayers on Au(111) surfaces; n is the number of molecules or radicals per model slab; ρ (nm^{-2}) the SAM density.

Thiol				Thiyl			
n	ρ	$\Delta G_{SH,g}(n)$	$\mu_{SH}(n)$	n	ρ	$\Delta G_{S,g}(n)$	$\mu_S(n)$
27	0.71	-228.4	-210.5	27	0.71	-371.6	-223.7
54	1.41	-206.8	-188.9	81	2.12	-316.0	-168.1
75	1.96	-116.0	-98.1	135	3.53	-244.4	-96.5
97	2.54	-117.9	-100.0	153	4.00	-182.3	-34.4
126	3.30	-101.4	-83.5	155	4.06	-144.1	+3.8
142	3.72	-88.2	-70.3	162	4.24	-85.2	+62.7
				185	4.84	+291.8	+439.7